

Authors' response and changes to the manuscript

- I would suggest precising the title to “Characterization of the unsteady aerodynamic response of a floating offshore wind turbine to surge motion”.

The title has been changed similarly to what suggested.

- Maybe it should be clarified early in the paper that whenever surge is mentioned, harmonic surge is considered. The adjective harmonic has been used more extensively when the imposed surge motion has been mentioned.

- Line 18: The variables in the equation should be introduced.

Corrected.

- Line 73: The bracket before “(Bayati et al., 2017b” should probably be moved “Bayati et al. (2017b”.

Corrected.

- Figure 2: Size should be increase for better readability.

The figure (now number 3) has been enlarged up to text width.

- Line 160: “i.e. all what attached” -> “i.e. all what is attached”.

Rephrased and corrected.

- Line 294: double “the”.

Corrected.

- Figure 7: Which test number or amplitude is shown?

The test number is specified in both the text and the caption.

- Line 310: a comma behind “both” is missing.

Corrected.

- Line 347: This sentences is hard to understand and should be rephrased: “The main cause of these oscillations is the turbulence that, albeit weak because of the smooth flow boundary condition at inlet, forms upstream the turbine because of both the high wind tunnel Reynolds number and the influence of the actuator forces in the rotor plane”.

The sentence has been rephrased.

- Line 449: “...coherent to what was observed for the thrust...”.

Rephrased and corrected.

- Figure 7a: In the raw WT timeseries a frequency double the surge frequency can be clearly seen. Please explain where this frequency originates and why it was filtered out. This is quite important as the good agreement between numerical codes and experiments would not be achieved otherwise. Furthermore, this is crucial to justify the implicit assumption that thrust variations due to surge have the same frequency of the surge variation made in section 4.2.2. The filtering procedure should also be explained in further detail as the signal was filtered quite significantly.

Section 4.2.1 has been updated, reformulating the comments on the unfiltered time history for better clarity (the details have been provided in the discussion).

- Conclusions: “The codes have all confirmed the aerodynamic response to be dominated by the component at the surge frequency. Hence, considering only that harmonic, it has been possible to clean the experimental measurements that were characterized by significant disturbances due to the unsteady tests’ complexity.” – Could it be possible that the numerical models are not able to capture phenomena observed in the experiments? Please elaborate on this point.

This point has been covered in the Authors' comment posted in the discussion.

- English should be checked thoroughly. For instance, the preposition “a” and the article “the” are often missing or used inappropriately.

The use of English has been extensively revised with the aid of a native speaker.

- Introduction: The authors mention that the developed test rig has 2 degrees of freedom: pitch and surge. This study seems to be focused only on surge however, can you explain this choice in more detail? Furthermore, since the work focuses on basic understanding of the aerodynamic phenomena & code performance, it would be useful to the uninitiated if an explanation of the most aerodynamically relevant platform motions are and perhaps a diagram refencing those motions. At the very least authors should provide references for the mentioned information.

Some sentences have been added in the introduction, along with a schematic figure, hoping to give a clearer picture of the topic to the uninitiated.

- The introduction also mentions the lack of the influence of floating dynamics on WT control. In this paper however pitch control is disabled. I suggest shortening the paragraph and only mentioning that the results are presented in the frequency domain as well that is useful for controller design.

That part has been shortened as suggested.

- Section 2.2: I find the names RATED1 and RATED2 confusing. Although they both refer to design TSR conditions, one refers to below-rated wind speeds. Controller behavior can be very different at rated and below rated. In accordance with the paper, I suggest the names to be changed to BELOW and RATED. I am open to other reasonable explanations.

The names have been changed as suggested.

- Line 175: Please revise the phrase “Both models are lifting line codes, i.e. they make use of aerodynamic look-up tables to evaluate airfoil performance.” The fact that a code uses aerodynamic look-up tables does not necessarily mean that it is a lifting-line code, actually BEM codes are typically not LL codes. If the specific code includes a lifting-line formulation for the blades and momentum modelling for the wake it should be clarified.

The sentence in question has been removed.

- Section 3.1 Please clarify the effects that are being modelled with engineering models in BEM. This is crucial for a fair comparison.

Sentences have been added in Section 3.1.3 to clarify this point.

- Section 3.1.3 Have the values discussed here been validated by means of a sensitivity analysis? Other authors have suggested much shorter timesteps and longer wakes to obtain independent results.

Sentences have been added in Section 3.1.3 to clarify this point as well.

-Section 3.2 The authors mention that a LES simulation was performed. Was the Pope criterion or similar criteria to verify that an adequate percentage of the turbulent spectrum was resolved verified?

As anticipated in the discussion, a sentence has been added to specify that the characteristic cell size was in the integral range of turbulence in the inflow.

- Section 3.3 How is the surge motion modelled in the CFD code? Please specify if automatic remeshing or grid deformation is applied or if there are rotating interfaces as sometimes seen when simulating rotors.

A sentence has been added to clarify this point.

- Figure 5: The authors might already be aware of this but it would be useful to include curves for the “full CFD” model a swell, to better highlight which model over-under estimates power & torque.

As explained in the discussion, the load distributions from the full CFD were not available unfortunately.

- Table 4: Please clarify the parameters f_s and A_s in the description.

Corrected.

- Figure 7: QS timeseries is had to make out, please choose another color.

Several alternative colors have been tested, but none of them gave a satisfactory result and thus the color has been left yellow. However, a different dash style has been employed to improve readability.

- Section 4.2.2 It seems to me that in the formulas 6 and 7 the dependency from $e^{(2\pi f_s t)}$ was omitted. Please clarify this point. The same considerations apply to eq. 19.

The term has been implied in the phasor representation and this has been specified in the text.

Characterization of the unsteady aerodynamic response of a floating offshore wind turbine to surge motion

Simone Mancini¹, Koen Boorsma², Marco Caboni², Marion Cormier³, Thorsten Lutz³, Paolo Schito¹, and Alberto Zasso¹

¹Politecnico di Milano, Department of Mechanical Engineering, Milano, Italy

²ECN part of TNO, Petten, Netherlands

³University of Stuttgart, Institute of Aerodynamics and Gas Dynamics, Stuttgart, Germany

Correspondence: Simone Mancini (simone1.mancini@mail.polimi.it)

Abstract. The disruptive potential of floating wind turbines has attracted the interest of both ~~industry and the industry and the~~ scientific community. Lacking a rigid foundation, such machines are subject to large displacements whose impact on ~~the~~ aerodynamic performance is not yet fully ~~acknowledged~~explored. In this work, the unsteady aerodynamic response to ~~an~~ harmonic surge motion of a scaled version of the DTU10MW turbine is investigated in detail. The imposed displacements

5 have been chosen representative of typical platform ~~motions~~motion. The results of different numerical models are validated against high fidelity wind tunnel tests specifically focused on the aerodynamics. Also, a linear analytical model, relying on the quasi-steady assumption, is presented as a theoretical reference. The unsteady responses are shown to be dominated by the first surge harmonic and a frequency domain characterization, mostly focused on the thrust oscillation, is conducted involving aerodynamic damping and mass parameters. A very good agreement among ~~codes, experiments and the codes, the experiments~~and the 10 quasi-steady theory has been found clarifying some literature doubts. A convenient way to describe the unsteady results in ~~a~~ non-dimensional form is proposed, hopefully serving as ~~a~~ reference for future ~~work~~works.

1 Introduction

Lacking a rigid foundation, floating offshore wind turbines (FOWTs) are subjected to large displacements during their operation. Therefore, ~~the~~ classical control strategies, suitable for bottom-fixed turbines, have to be redesigned accounting for 15 these motions. The application of an inland turbine controller to a FOWT might lead, indeed, to dangerous controller induced resonances (Nielsen et al., 2006). Moreover, ~~Sebastian and Lackner (2013) pointed out that~~ floater displacements can be a major source of aerodynamic unsteadiness, because their typical periods are comparable to the time scale of dynamic inflow phenomena ($\tau = D/V_0$, with τ being the time scale, D the rotor diameter and V_0 the free stream wind velocity). Since the 20 design of a FOWT controller cannot prescind from ~~an~~ accurate inflow modelling (Pedersen, 2017), the presence of dynamic inflow effects due to platform motions requires a detailed investigation.

~~Depending on the type of floater, different~~ The six degrees of freedom (D.o.F.) ~~are more excited than others. For example, of a~~ FOWT are shown in Fig. 1. Analysing different types of platforms, ~~Sebastian and Lackner (2013) showed that the most excited modes depend on the floater configuration. However, owing to the usual alignment between the wind and the waves, pitch and~~

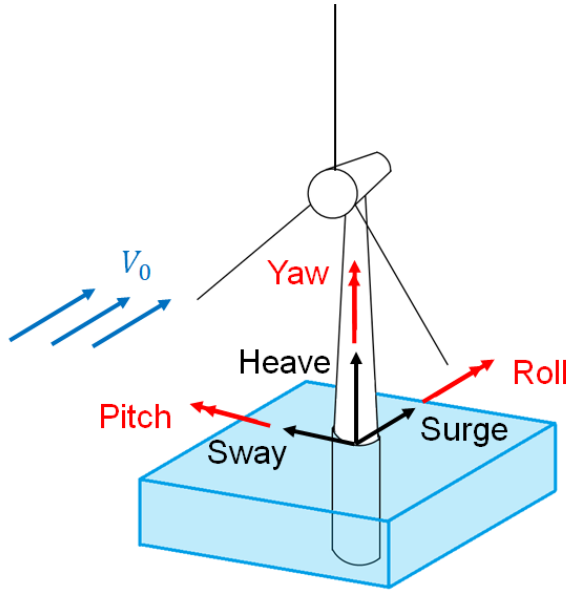


Figure 1. Sketch of the six degrees of freedom of a FOWT.

surge motions are typically the most significant (Mantha et al., 2011). In particular, spar types of floaters (e.g. HYWIND™) are

25 more prone to pitching, whilst both semi-submersible (e.g. WindFloat®) and tension-leg platforms (TLPs) are less affected by pitch oscillations than spar type floaters (e.g. HYWIND™). However, owing to the typical alignment between wind and waves, platform surge is commonly one of the most significant modes particularly affected by surge oscillations that also drive the tensile load on the mooring lines (Madsen et al., 2020). In addition, small turbine pitch rotations are often approximated to surge motions by means of linearization. Despite linearized to surge displacements to simplify the aerodynamic modelling,

30 Even if the simple kinematics ~~consents~~ allows the use of the momentum theory with little modifications, it is still unclear whether current blade element momentum (BEM) codes can adequately model FOWT the aerodynamic response to ~~surge~~ the surge of a FOWT. In fact, neither the impact of unsteady effects nor the accuracy of current engineering dynamic inflow models are uniquely acknowledged for this case.

Several numerical studies addressing the impact ~~The influence~~ of surge motion on turbine performances have been conducted.

35 Regardless ~~the~~ the performance of a floating turbine was addressed by several numerical studies. Regardless ~~of~~ the common benchmark provided by the NREL's 5MW reference wind turbine (RWT), the results led to rather discordant conclusions. Studying ~~characteristic floater motions~~ the characteristic floater motion with a free vortex wake (FVW) code, Sebastian and Lackner (2012) underlined the need of higher fidelity models than BEM. Conversely, de Vaal et al. (2014) found that surge displace-

40 ments, in the typical frequency range of a TLP, were slow enough for dynamic inflow effects to be insignificant. Such a conclusion was drawn comparing a moving actuator disk (AD) to both a quasi-steady BEM and another BEM with ~~the~~ Øye's dynamic inflow model (1990) implemented. At a similar frequency though, Micallef and Sant (2015) found relevant differ-

ences ~~among~~ between BEM, generalized dynamic wake (GDW) and AD model results. They also noticed that ~~the~~ unsteadiness increased with the tip speed ratio (λ). ~~This, which~~ was confirmed by a FVW code too (Farrugia et al., 2016). The most detailed work on the aerodynamic ~~effects~~ effect of surge was performed by Tran and Kim (2016), who were the first to adopt a full CFD model for the purpose. Considering similar surge cases to de Vaal et al., they solved the RANS equations with a $k - \omega$ SST model featuring an overset mesh technique; the results were then compared against a BEM ~~code~~ with Øye's model and a GDW solver. The discrepancies at the highest frequencies and amplitudes ~~aroused doubts on~~ introduced doubts about possible dynamic inflow effects. Unfortunately, ~~none in all~~ of these studies ~~addressed closely the theme of control, limiting the analysis, the analysis was limited~~ to the time domain. ~~From the controller design point of view though, the characterization of load signals in terms of amplitudes and phases in frequency domain is fundamental because it allows to evaluate~~ In the present work instead, the results are also presented in the frequency domain determining control-relevant parameters like the aerodynamic damping (c_{aero}), which rules ~~the~~ system dynamics in surge. ~~One of the few works linking FOWT control and unsteady aerodynamics due to platform motions was that of Lennie et al. (2016), but the aim was other than spotting the influence of dynamic inflow. In fact, it studied the effects of a feathering blade pitch actuation during turbine pitch motion (approximated to surge) by means of a FVW model.~~

~~Also the~~ The lack of experimental data for ~~code validation~~ codes validation also hampered a clear understanding of dynamic inflow effects due to surge. Most of the available works involved Froude scaled models, tested in water basins equipped with fans to reproduce the wind. Apart from some tests on very small turbines (Farrugia et al., 2014; Sant et al., 2015; Khosravi et al., 2015), from which it was hard to draw any full-scale conclusion, a validation campaign on a 1:60 scaled version of the NREL5MW RWT was conducted by Ren et al. (2014), but the interest was mainly on the hydrodynamic loading and ~~surge was considered as~~ the surge motion was considered an output. ~~At MARIN's offshore basin Goupee et al. (2017) carried out intensive testing of a 1:50 model of the NREL5MW, mounted on a semi-submersible platform, specifically focusing on control aspects. More recently, Madsen et al. (2020) performed similar experiments on a 1:60 model of the DTU10MW RWT mounted on a TLP, investigating the system's response to various wind and waves conditions with different control strategies~~ Similarly, Goupee et al. (2017) and Madsen et al. (2020) carried out plenty of tests to address the impact of the control strategy on the motion of different platforms. Nevertheless, it is very difficult to understand the influence of ~~the~~ unsteady aerodynamics from combined wind and waves tests. For this reason, Polimi decided to focus more specifically on the aerodynamics, aiming both at an increased comprehension and at the generation of valuable data ~~for codes to serve as a benchmark for code~~ validation. For ~~the this~~ purpose, a 1:75 model of the DTU10MW RWT was designed within ~~the project LIFES50+ project~~ (Bayati et al., 2017a, c). The scaled turbine was mounted inside Polimi's wind tunnel (GVPM) on a two D.o.F. test rig ~~allowing to impose that allowed the imposing of~~ both pitch and surge motions. The first experiments conducted seemed to show relevant traces of unsteady effects due to surge (Bayati et al., 2016). However, after a thorough revision, it was understood that the results had been strongly biased by ~~the~~ tower flexibility. Therefore, a stiffer tower was manufactured to run new harmonic surge tests in ~~the~~ project UNAFLOW.

UNAFLOW (UNsteady Aerodynamics for FLOating Wind) was a collaborative project, belonging to the EU-IRPWIND program, ~~that which~~ involved four research institutions: POLIMI, ECN (now ~~part of~~ TNO), USTUTT and DTU. It focused on

advanced aerodynamic modelling and novel experimental approaches for studying the unsteady behaviour of multi-megawatt floating turbine rotors (2018). The work, carried out between June 2017 and April 2018, was divided in two work packages: the first studied the 2-dimensional airfoil aerodynamics ~~from by conducting tests in the~~ DTU Red wind tunnel~~tests~~; the second 80 focused on the scaled ~~model performances under imposed surge motion~~turbine model performance under imposed harmonic surge motions, comparing GVPM experiments with numerical ~~simulations~~results. The numerical part involved a full CFD model, provided by USTUTT, plus a BEM and a free vortex code (AWSM) provided by TNO. Input to the lifting line codes were the airfoil polars obtained in the first work package. The significant amount of data generated within UNAFLOW was made available to the scientific community, including a number of steady and unsteady tests on ~~a~~ SD7032 airfoil, steady and 85 unsteady full turbine loads, and PIV wake measurements. ~~Later~~The latter were investigated by ~~(Bayati et al., 2017b, 2018b)~~Bayati et al. (2017b, 2018b) and an overview of the main results ~~was given~~can be found in Bayati et al. (2018a). Concerning ~~the~~ CFD results, only those obtained with the axisymmetric model were ~~published~~addressed in Cormier et al. (2018) and included 90 in the final project report (2018). Moreover, an inconsistency in the set up of ~~several~~some simulations was later discovered, explaining the large discrepancies found in the comparison. For this reason, ~~a complete results revision and update has been recently conducted to reach~~the results have been recently reviewed and updated reaching a final convergence (Mancini, 2020).

In this work, the latest comparison of the turbine ~~performances during~~performance under harmonic surge is presented. 95 ~~Diversely from~~With respect to the original UNAFLOW report (2018): the unsteady thrust response from wind tunnel measurements has been obtained with a revised inertia subtraction procedure; the full CFD results have been included, together with new BEM and AWSM simulations; the outcomes of an Actuator Line code (AL) have been added as an intermediate fidelity level. A frequency domain analysis has been performed focusing on control-relevant quantities, and the influence of ~~surge motion's~~the amplitude and frequency of the surge motion has been investigated. To have a theoretical reference, a simple linear model based on quasi-steady theory (Appendix A) has also been included in the comparison. In attempt ~~of giving~~to give a more general representation to the unsteady analysis, the results in the frequency domain have been reported in a non-dimensional form, defining some meaningful parameters that may be ~~used conveniently in future work~~conveniently used in future works. This paper aims to shed light on the ~~surge induced~~surge-induced unsteady aerodynamics of a FOWT, providing the first publicly available experimental data to be used as a benchmark for codes validation. The main research goal was to reach a clearer awareness on the impact of dynamic inflow effects. As ~~side benefits, also a side benefit~~, a valuable comparison ~~among the different fidelity models for wind turbine aerodynamic modelling~~of some state-of-the-art codes for the aerodynamic modelling of wind turbines has been produced, along with a robust ~~result nondimensionalization strategy have been produced~~nondimensionalization strategy for the results.

2 Wind tunnel tests

The turbine model tested in UNAFLOW was a 1:75 scaled version (2.38 m diameter) of the DTU10MW RWT. Such ~~a~~ reference rotor was chosen to resemble the size of current offshore units being installed. The model was completely designed and engineered by Politecnico di Milano within LIFES50+, ~~pursuing an accurate match of~~accurately matching the RWT aerody-

Table 1. Key parameters of the DTU 10MW compared to [the](#) Polimi's model.

	DTU10MW RWT	Polimi model
Control	Variable speed + Collective pitch	Variable speed + individual Individual pitch
Drivetrain	Medium Speed, multiple stage gearbox	Transmission belt, epicyclic gearbox
Gearbox ratio	50	42
Diameter	178.3 m	2.38 m
Hub height	119 m	2.05 m
Tilt angle	5 °	5 °
Coning angle	-2.5 °	0
Blade prebend	3.33 m	0

110 namic coefficients, [especially](#) [the](#) thrust coefficient (C_T) [espeially](#), because of the leading role of thrust in the dynamics of a FOWT. Whilst in Froude scaled models (e.g. Goupee et al., 2017; Madsen et al., 2020) [the blade pitch is typically adjusted](#) in order to cope with the steady thrust reduction due to lower Reynolds [the blade pitch is typically adjusted](#)[numbers](#), here a different approach was followed for [a](#) better aerodynamic accuracy. [Provided](#)[Given](#) that the dimensions were scaled by a factor [of](#) 75 to fit in the wind tunnel and the wind velocity was scaled by a factor [of](#) 3 for surge actuation purposes, the Reynolds 115 number was 225 times lower than [in](#) reality. Hence, a low Re profile (SD7032) was employed [changing, changing the](#) chord and twist distributions to fulfill the loads compliance. Such [proeedure allowed to achieve a](#) [procedure allowed](#) an accurate thrust reproduction throughout the whole operating range, [together along](#) with a satisfactory torque match up to rated [wind](#) conditions (Bayati et al., 2017c). The scaled turbine was also equipped with variable speed and individual blade pitch controllers (Bayati 120 et al., 2017a), but these features were not exploited in [the unsteady](#)[these](#) tests. In Table 1 the key characteristics of the scaled turbine are compared to those of the RWT.

The experimental campaign was carried out in the Boundary Layer Test Section of the GVPM (13.84 m wide x 3.84 m high x 35 m long). The tests were performed in [a](#) empty inlet configuration (i.e. without roughness elements or turbulence generators) [, aiming to obtain an inflow velocity profile as constant as possible. Figure 2 shows the resulting wind speed and turbulence intensity \(T.I.\) distributions measured 5 m upstream \[of\]\(#\) the rotor plane and normalized by the value measured at \[the\]\(#\) hub height. The wind speed could be considered constant in the rotor zone with a T.I. \[of\]\(#\) around 2 %.](#)

2.1 Experimental set-up

The model turbine was mounted on a slider, [commanded](#)[which was operated](#) by means of [an](#)[a](#) hydraulic actuator to produce the desired surge motion, as shown in Fig. 3; a schematic sketch with the reference system adopted in this work is also included. Another hydraulic piston was connected to a slider-crank mechanism underneath the tower, which allowed [to control](#)[the control](#) 130 [of the](#) turbine pitch too. However, [the](#) latter feature was not exploited in UNAFLOW and the mechanism was only used to place

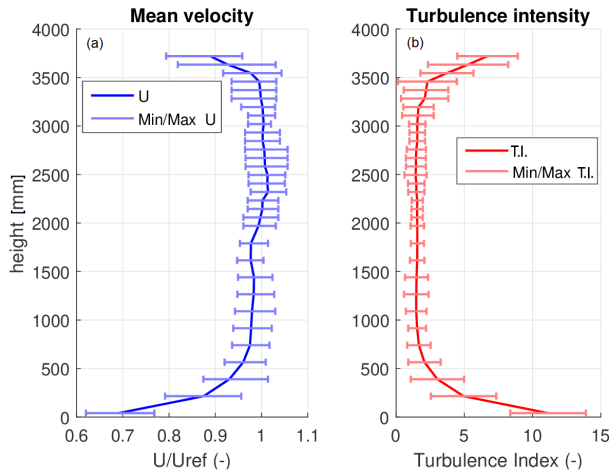


Figure 2. Wind tunnel speed and T.I. profiles normalized by the value measured at hub height with error bars.

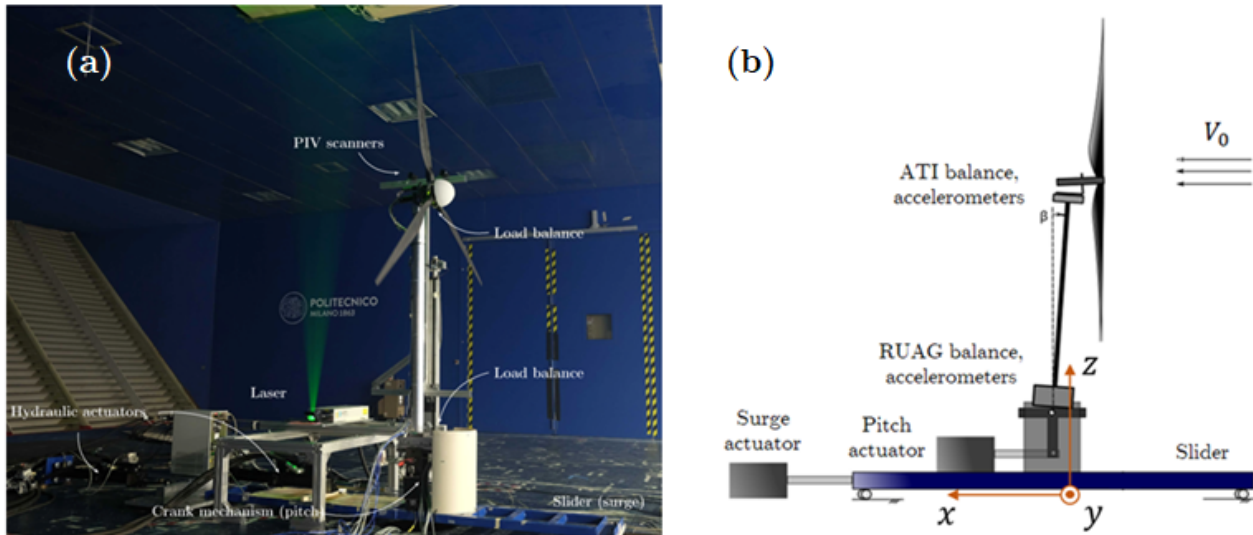


Figure 3. Experimental setup picture (a) and schematic sketch with the reference system (b).

the rotor perpendicular to the inflow (i.e. to cancel the 5° design tilt angle). This choice was made to avoid the ~~periodic effects related~~ periodic effects.

A wide array of sensors was employed to measure both ~~the~~ dynamic response and ~~the~~ flow field characteristics. All the instruments were synchronized and ~~everyone~~ all of them sampled at 2 KHz. The shaft was equipped with an encoder and a proximitor, ~~measuring which measured~~ the rotational speed and ~~the~~ azimuthal position respectively. Loads were measured by means of two six-components balances ~~mounted one~~, one mounted at the tower base (RUAG) and one underneath the nacelle

Table 2. Operating conditions tested in UNAFLOW.

	V_0 [$m s^{-1}$]	Ω [rpm]	λ [-]	θ_p [$^\circ$]
RATED1 BELOW	2.5	150	7.5	0
RATED2 RATED	4.0	241	7.5	0
ABOVE	6.0	265	5.5	12.5

TBN: BELOW and RATED tests are called respectively RATED1 and RATED2 in the project report 2018

(ATI); only the latter was used in the post-processing. A couple of accelerometers was Two accelerometers were placed next to each balance: at the base they measured along the surge and heave directions (x and z according to Fig. 3b); at the nacelle along they measured along the surge and sway directions (x and y). To measure base's surge position the surge position of the 140 base, both an LVDT and a laser transducer were placed. The laser was chosen as the reference measure for its lower delay. For what concerns the flow field, the incoming wind speed was measured by a Pitot tube located 5m upstream of the turbine at a height of 1.5 m from the floor. The PIV system consisted of a pair of cameras mounted on an automatic traversing system and connected to an Nd:Yag laser, which enlightened the seed particles in the flow. The pictures were post-processed with PIVview 3C (PIVTEC) to create the 2D velocity contours in various zones of the near wake. This However, this work focuses on the 145 aerodynamic loads and the wake measurements, despite being tightly linked, will not be considered.

2.2 Steady tests

Before imposing the surge motion, steady tests were carried out at three different wind speeds obtaining the reference sealed model's stationary performances to obtain the reference static performance. The operating conditions considered are reported in Table 2. The first two cases (named RATED1 and RATED2 ~~BELOW and RATED~~) were both at the optimal tip speed ratio 150 ($\lambda = 7.5$), with the blades in the neutral pitch position, but with different wind velocities (variable speed rotor). The ABOVE case instead, considered an above-rated wind speed with a lower λ and a blade pitch of 12.5° towards feather.

2.3 Unsteady tests

For all each of the three steady conditions, a number of unsteady tests was performed. An were performed. A hydraulic actuator was used to impose a sinusoidal surge motion to the slider upon which the turbine was mounted. The displacement at the base 155 of the tower could be expressed as:

$$x_B(t) = A_s \sin 2\pi f_s t; \quad (1)$$

being with A_s and f_s being the surge amplitude and frequency, respectively. Different pairs of amplitude and frequency values were tested. Being the platform surge of a FOWT induced by the hydrodynamics, the frequency range of the motion depends on the waves excitation. Therefore, different f_s values were chosen to represent possible frequencies at which a peak in the

160 sea waves spectrum might be found. The selected range went from 0.125 Hz to 2 Hz ~~in-at~~ model scale, corresponding to $0.005 \leq f_s^{real} \leq 0.08$ Hz ~~in-at~~ full scale. ~~The range was totally~~ ~~This range was~~ consistent to those investigated in ~~the~~ literature (de Vaal et al., Micallef and Sant, Farrugia et al. and Tran and Kim). Provided that ~~the~~ real turbine oscillation amplitudes depend on the floater type and on ~~site-specific~~ ~~site-specific~~ parameters (e.g. water depth and mooring lines), different A_s ~~values~~ were considered at each frequency so as to cover a wide range of possibilities. The amplitude range selected guaranteed the 165 magnitude of the angle of attack variation in surge to be limited, confining dynamic stall effects to the blade root only. A total of 84 unsteady tests ~~was-were~~ conducted, 28 for each steady operating condition. The full test matrix can be found in Bernini et al. (2018). It is important to observe that, ~~during surge~~, the standard turbine controller was not active ~~during surge~~, and both the blade pitch and the rotational speed were kept constant at the values reported in Table 2.

170 One of the major challenges of the experimental campaign was the extraction of the aerodynamic thrust from the balance measurements. In fact, especially at the higher f_s , the load signal was heavily affected by ~~the~~ nacelle inertial contribution ~~caused~~ ~~by~~ ~~due to~~ the imposed surge acceleration. Originally the inertia subtraction was made assuming a perfectly rigid system: the aerodynamic part ~~was-extracted~~ ~~of the signal was extracted by~~ subtracting from the force ~~signal~~ measured during surge, the ~~force measurement obtained with one measured imposing~~ the same surge motion ~~but~~ without wind. Tests without wind were referred to as NOW (i.e. NO-Wind). Mancini (2020) showed that the high aerodynamic damping, ~~generated by the rotor~~ 175 when the wind was active, ~~had led to dynamic amplification effects~~ ~~that, which had~~ biased LIFES50+ results. The stiffer tower employed in UNAFLOW was proven able to mitigate such effects. ~~However~~ ~~Anyhow~~, an alternative inertia subtraction procedure capable of reducing the bias due to ~~tower~~ flexibility was proposed and it has been used in this work. Having the acceleration measure ~~in-along~~ ~~x direction~~ (Fig. 3b) at the nacelle, the aerodynamic thrust force has been obtained as:

$$T(t) = F^{ATI}(t) + m ACC(t); \quad (2)$$

180 ~~being~~ ~~with~~ ~~T~~ ~~being~~ the aerodynamic thrust, ~~whilst~~ ~~and~~ F^{ATI} and ACC ~~respectively~~ the ATI balance ~~'s~~ and the accelerometer ~~'s~~ measurements along x , ~~respectively~~. The mass of the nacelle (m), i.e. all ~~what~~ ~~that was~~ attached to the ATI balance, has been estimated from the NO-Wind tests considering the amplitudes of the surge frequency harmonics extracted through a Fast Fourier Transform:

$$m = \frac{|F_{NOW}^{ATI}|_{@f_s}}{|ACC_{NOW}|_{@f_s}}. \quad (3)$$

185 A comparison among different inertia subtraction procedures can be found in Mancini (2020).

In order to avoid leakage in the frequency domain analysis ~~all~~, ~~all the~~ wind tunnel test signals have been windowed, always considering six full surge periods.

3 Numerical codes description

Four different numerical methods have been used for ~~a~~ numerical-experimental cross validation: a BEM and a FVW (AWSM) 190 part of ~~the~~ ECN's Aero Module (Sect. 3.1), an AL (Sect. 3.2) and a full CFD model (Sect. 3.3). The codes have been selected

to cover almost the whole ~~state-of-art~~ ~~state-of-the-art~~ fidelity range available for ~~wind-turbine-aerodynamic-modelling~~ ~~the aerodynamic modelling of wind turbines~~. This way it is possible to better understand the capability of each method to deal with ~~the~~ unsteady aerodynamics.

3.1 Aero Module

195 The ECN Aero-Module (Boorsma et al., 2011, 2016, 2020) contains two aerodynamic models, namely the Blade Element Momentum (BEM) method similar to the implementation in PHATAS (Lindenburg and Schepers, 2000) and a free vortex wake code in the form of AWSM (van Garrel, 2003). Both models ~~are lifting line codes, i.e. they make use of~~ ~~use~~ aerodynamic look-up tables to evaluate ~~the sectional~~ airfoil performance. Several dynamic stall models, 3D correction models, wind ~~modeling~~ ~~modelling~~ options and a module for calculating ~~tower effects~~ ~~the tower effect~~ are included. The set-up allows to easily switch
200 between the two aerodynamic models whilst keeping the external input the same, which is a prerequisite for a good comparison between them.

3.1.1 Wake ~~modeling~~ ~~modelling~~

Since a pure BEM code only resolves the rotor plane, an engineering model has to be added to simulate wake effects. Therefore, the ECN dynamic inflow model (Snel and Schepers, 1994) has been implemented to account for the aerodynamic rotor
205 ~~inertia~~. The dynamic inflow model adds another term to the axial momentum equation. This term is proportional to the time derivative of the annulus averaged axial induction of the element under consideration and its magnitude varies with the radial position.

AWSM, ~~instead~~, uses the blade geometry to create vortex lattices which are convected in the wake, conserving ~~shed and the~~ ~~shed and the~~ trailing vorticity as depicted in Fig. 4. ~~Here the~~ ~~The~~ trailing vorticity accounts for the ~~effects of~~ spanwise circulation variation, whilst the shed vorticity accounts for the ~~effects of bound vortex~~ variation with time. ~~Consequently all of~~ ~~the bound vortex. Consequently, all the~~ wake related flow phenomena (e.g. dynamic inflow, aero-elastic instabilities featuring shed vorticity variation and skewed wake effects) are ~~modeled~~ ~~modelled~~ intrinsically, where they are covered by engineering models or not covered at all in BEM. If the wake points are ~~modeled~~ ~~modelled as~~ free, the convection of each wake point is determined by the aggregate of the induced velocities from all vortices using the ~~Biot and Savart~~ ~~Biot-Savart~~ law.

215 3.1.2 BEM implementation in surge

A turbine subjected to surge or pitching ~~motion~~ ~~motions~~ experiences apparent wind velocities at the rotor due to the movements of the tower base. Since these wind velocities add energy to the system (as they are induced by the waves), it can be argued ~~to incorporate these that these should be incorporated~~ in the effective wind speed used in the momentum part of the BEM equations. This in addition to the obvious implementation of ~~this~~ ~~such~~ relative motion in the element part of the BEM equations.
220 The validity of this statement ~~is verified by~~ ~~has been verified~~ comparing a simulation ~~in surge~~ with a moving rotor (which is used in the present work) to a simulation with a 'fixed' rotor featuring a ~~(sinusoidal)~~ ~~sinusoidal~~ wind variation in agreement

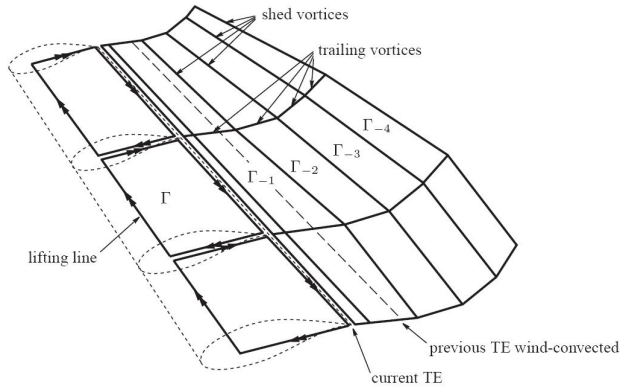


Figure 4. AWSM wake geometry (van Garrel, 2003).

with the surge motion. Free vortex wake simulations give nearly identical results for both approaches in this case, indicating that the main effect the wind turbine rotor experiences is the apparent wind effect rather than the rotor moving into and out of its own wake. For the BEM simulations it ~~is has been~~ observed that the shape of the force response is ~~off inconsistent~~ if apparent wind velocities are not taken into account in the momentum equations.

225 ~~Implementation-wise~~ ~~Implementation-wise~~, this can result in a challenge since an aero-elastic code is not always aware ~~whether motion of the blade of whether the blade motion~~ is due to ~~flexible nature of the turbine~~ ~~the turbine flexibility~~ (e.g. tower fore-aft bending) or due to ~~the~~ platform motion induced by waves. Recommended practice here is to register ~~the~~ translational and rotational movement at the tower base and extrapolate the resulting apparent wind velocities to the ~~designated~~ rotor plane 230 locations ~~of interest~~. For a pitching movement this would imply a linear variation with height of ~~the~~ apparent wind velocity over the rotor disk, and hence a non-uniform inflow condition, which anyhow is a challenge for BEM simulations.

3.1.3 Aero Module settings

235 ~~A~~ ~~To be consistent with the higher fidelity models, a~~ rigid version of the turbine has been simulated. The airfoil data have been obtained from the corresponding 2D experiment in UNAFLOW (Bernini et al., 2018) for clean conditions at a Reynolds number of $1 \cdot 10^5$. The ~~Snel's~~ 3D correction (Snel et al., 1993) has been used to account for rotational effects on the airfoil data. Also, the first order dynamic stall model of Snel (1997) has been employed in all the simulations. The effect of tower stagnation has not been included instead. The time step has been kept at the approximate equivalent of 10° azimuth for both the BEM and AWSM simulations. ~~The Snel dynamic stall model (Snel, 1997) has been applied to all simulations, which has proved small enough to capture the surge motion and the related unsteady effects under investigation.~~

240 For the free vortex wake ~~simulation~~ simulations, the number of wake points has been chosen to make sure that the wake length developed ~~ever for~~ at least three rotor diameters downstream of the rotor plane. The wake convection has been set free for approximately two rotor diameters ~~downstream~~. ~~For the remaining diameter, then for the remaining part~~ in the far wake, the blade average induction at the ~~free-to-fixed wake transition is~~ ~~free-to-fixed wake transition has been~~ applied to all ~~the~~

245 downstream wake points. These settings were shown to keep the average torque and thrust levels within a small percentage of a reference simulation featuring 25 rotor diameters wake length, while the dynamic loading appeared not to be affected at all.

3.2 Actuator line

The actuator line model has been chosen as an intermediate step between the free vortex method and the full CFD. To run the simulations, a MECC's (Polimi) in-house developed actuator line code for OpenFOAM (2011) has been used. Diversely from In contrast with a classical actuator line, such code adopts an effective velocity model (EVM), as proposed by Schito and 250 Zasso (2014), to evaluate the relative velocity vector used in the calculation of the aerodynamic forces. In particular, instead of evaluating it at the very same point where the force is applied, the EVM considers a series of sampling points along a line, placed perpendicularly to the wind and upstream of the profile leading edge, and estimates estimating the relative velocity as a vectorial average among the samples. This technique was successfully employed to model the aerodynamics of vertical axis turbines (Schito et al., 2018; Melani et al., 2019). Thanks to the EVM, the smearing parameter of the Regularization Kernel 255 function (a bi-variate normal distribution) has been set equal to the characteristic cell size without problems of numerical stability. The length and position of the sampling line has followed have been chosen according to the optimal values reported in Schito and Zasso (2014). Furthermore, the code has provided indicated by Schito and Zasso (2014). The code gives the possibility of imposing a surge motion to the actuator lines for replicating and this has been exploited to replicate the unsteady wind 260 tunnel tests. The airfoil polars that have been used for AL are the same adopted in as in the Aero Module simulations and the spanwise chord and twist distributions have followed the sealed model's specifies. Only the three blades have been considered modelled (as rigid actuator lines); neither the tower nor the nacelle have been taken into account.

The computational domain has reproduced faithfully the wind tunnel section 's-width and height. The streamwise direction has been modified setting the inlet section 5 m upstream of the turbine, i.e. where the wind velocity was measured, and the 265 outlet more than six diameters downstream, to allow the for atmospheric pressure recovery. The walls have been assumed smooth to avoid the need of modelling the boundary layers. Thanks to the absence of the turbine, a completely structured and incoming flow aligned grid has been generated. Cubic elements have been used in the rotor zone and two cylindrical refinement zones have been set around the turbine. The detailed grid layout can be found in Mancini (2020). The chosen mesh has had almost 270 3.5 millions of cells, with 50 elements per actuator line and a characteristic cell dimension within the integral range of the inflow turbulence. Using a finer grid (11.6 millions elements, 75 per blade line) with the same layout, the average steady turbine loads have varied of have varied less than 1 %.

Thanks to the absence of boundary layers, Large Eddy Simulations (LES) have been conducted to solve the incompressible 275 Navier-Stokes equations, featuring the standard Smagorinsky model. More complex sub grid scale models could have been selected but Sarlak et al. (2015) proved their impact small, provided that a sufficient grid refinement is present. A third order QUICK scheme has been used for the convective term, with an almost purely second order Crank-Nicolson scheme for the time derivatives. The solver is based on the PISO algorithm, using a multi grid linear solver for the pressure and a preconditioned bi-conjugate gradient method for the velocity components. The time step size ($\Delta t = 0.0005$ s) has been selected in order to:

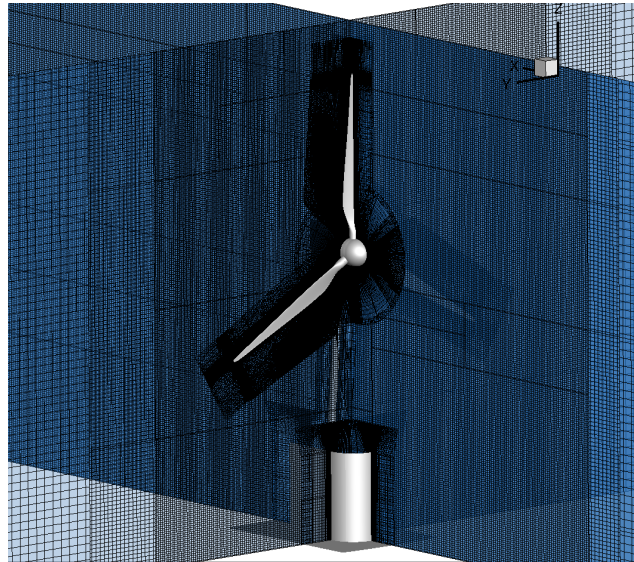


Figure 5. Numerical setup of the fully-resolved wind turbine (CFD).

keep the Courant number below 0.5~~to~~ prevent actuator line tips from crossing more than one cell per time step~~; avoid, and avoid the~~ leakage in the frequency domain analysis.

3.3 CFD

280 The fully-resolved CFD simulations have been run for a subset of cases to get more insights into the flow physics. The finite-volume flow solver FLOWer, originally developed by the German Aerospace Center, has been used for the present study (Kroll and Faßbender, 2005).

The computational setup of the ~~one-third-one-third~~ model of the scaled wind turbine, presented in Cormier et al. (2018), has been extended to a full model of the wind turbine as ~~represented shown~~ in Fig. 5. The compressible unsteady Reynolds-285 Averaged Navier-Stokes equations have been solved, using the Menter's shear stress transport model ~~to model the turbulence for turbulence modelling~~ (Menter, 1994). A second order dual time-stepping scheme has been ~~used employed~~ for the time discretization and ~~combined with~~ a multigrid algorithm ~~has been applied~~ to accelerate the convergence. The 5th order Weighted Non Oscillatory (WENO) scheme has been used for ~~the~~ spatial discretization in the wake of the wind turbine, in order to reduce the dissipation of the vortices (Kowarsch et al., 2013). In the body meshes and outside the wake region, ~~the~~ spatial 290 discretization has been realised with the 2nd order Jameson-Schmidt-Turkel (JST) scheme (Jameson et al., 1981). All ~~body component~~ grids have been embedded in a Cartesian background mesh ~~thanks to the Chimera grid overlapping technique by means of the Chimera overlapping mesh technique. Thanks to this technique, relative motions between the components and the background grid can be realized allowing the simulation of both the rotation of the rotor attached to the fixed tower and the surge motion of the whole turbine.~~ The hub has been extended from a 120 ° to a 360 ° section and new meshes for the

295 tower and its base have been generated. The grids have been ~~generated~~created with the commercial tool Pointwise, combined with in-house automatising scripts. The height of the first boundary layer cell in the body meshes has been chosen such that $y^+ \approx 1$ is ensured. The resulting numerical setup consists of 118 ~~Mio.~~millions cells. As the experimental streamwise velocity profile upstream ~~of~~ the turbine presented no shear in the rotor area, a uniform inflow has been applied at the inlet via a far-field boundary condition. To take into account the blockage effect ~~of the wind tunnel's due to the~~ upper and lower walls ~~of the wind~~
300 ~~tunnel~~, while optimizing the use of computational resources, the ceiling and ~~the~~ ground have been ~~modeled~~modelled by a slip boundary condition ~~, taking care to add as in AL simulations, but adding~~ a displacement thickness of 12.5 cm to meet the experimental flow rate. The distance between the wind turbine and the boundaries of the computational box has been defined according to Sayed et al. (2015), ~~who studied the influence of the distance to boundaries on the wind turbine aerodynamics~~. The outlet and ~~the~~ lateral boundary conditions have been set as far-field ~~too and located respectively and located~~ 9 and 5 rotor
305 radii away from the wind turbine, ~~respectively~~. A time step corresponding to a blade rotation of 1 ° with 60 inner iterations has been applied.

4 Results

Since dynamic inflow effects are known to be more relevant when the turbine loading is high, ~~it has been decided to focus the comparison~~ the comparison has been focused on rated wind conditions rather than above-rated. Furthermore, ~~RATED2~~
310 ~~RATED~~ tests (see Table 2) have been preferred to ~~RATED1~~BELOW ones because of the better ~~signal to noise~~signal-to-noise ratio characterizing the measurements.

4.1 Steady comparison

The steady ~~performances~~performance of the scaled turbine ~~are~~have been considered first, comparing the predictions of the different codes against the experiments without surge. The outcomes of this comparison are reported in Table 3, in terms of ~~the~~
315 steady thrust force (T_0) and mechanical power (P_0); the percentage errors have been defined with respect to ~~the~~ wind tunnel measurements. To run the steady CFD simulations, only the axisymmetric model (~~called here referred to as~~ 1/3 CFD) has been used. However, the good agreement found with the quasi-steady theory (Sect. 4.2) ~~, has given trust on estimating the steady~~
320 ~~performances~~performance from the full CFD model (~~called referred to as~~ CFD in Table 3), averaging the unsteady loads over a full surge period. The consistency of this approach has been confirmed by the excellent match with ~~the~~ steady wind tunnel tests, showing maximum discrepancies below two percent. The confidence has been raised further by the fact that the average values obtained from the two different surge simulations are almost ~~coincident~~identical.

Similarly to the full CFD, ~~also~~ the actuator line results are in very good agreement with ~~the~~ experiments. The Aero-Module codes (BEM and AWSM) show ~~more relevant discrepancies instead, higher discrepancies~~ especially for the power(*i.e.* torque) ~~that is underestimated of~~, ~~which is underestimated by~~ about 10 % by both models. The thrust is underrated as well, but to
325 a lower extent. Very similar values have been obtained by the axisymmetric CFD simulation too; hence BEM, AWSM and 1/3 CFD results are in good agreement among each other, but systematically different ~~than~~from the full CFD, ~~AL and the~~

Table 3. Comparison of the steady turbine model ~~performances~~ ~~performance~~ in ~~RATED2~~ ~~RATED~~ conditions.

	WT	CFD	AL	1/3 CFD	AWSM	BEM
T_0 [N]	35.91	36.57	36.60	34.20	35.00	34.65
error T_0	/	+1.84 %	+1.92 %	-4.76 %	-2.53 %	-3.51 %
P_0 [W]	83.79	84.29	87.07	73.44	75.5	73.95
error P_0	/	+0.6 %	+3.92 %	-12.35 %	-9.89 %	-11.75 %

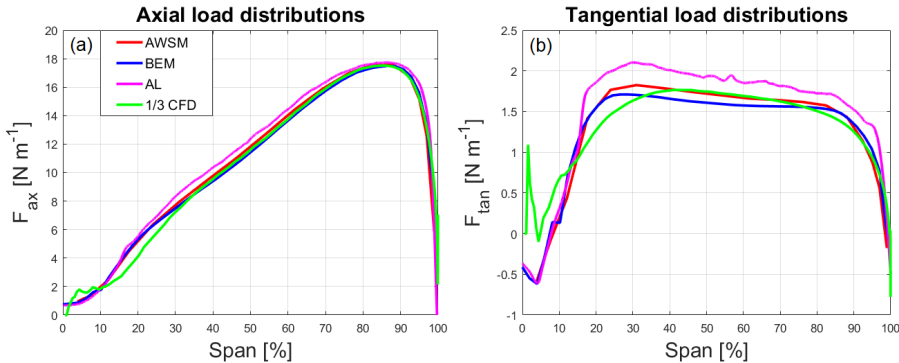


Figure 6. Axial and tangential spanwise loads distributions comparison.

~~AL and the~~ experimental tests. A significant source of this discrepancy appeared to be a ~~slight difference in inflow velocity~~ ~~small difference in the inflow velocity~~, due to the fact that the reference wind speed ~~in~~ ~~of~~ wind tunnel tests was measured 5 m upstream of the rotor, where the induction field had ~~indeed an impact, albeit small, and this a slight impact that~~ was not accounted ~~for~~ by all the models. However, the influence of such discrepancy on the unsteady investigation is expected to be negligible.

To deepen the steady comparison, the spanwise ~~loads~~ ~~load~~ distributions obtained with the different codes have been considered. In Fig. 6 the axial and tangential, i.e. contributing to thrust and torque respectively, unit ~~forces~~ ~~force~~ distributions along the span are reported. Unfortunately, the spanwise distributions from CFD have been extracted from the steady axisymmetric simulation only. ~~For what concerns the the~~ ~~In regards to the~~ axial load (Fig. 6a), the shape is the same for all the models and the discrepancies are small throughout the ~~whole~~ span. In accordance to the integral values, the match among BEM, AWSM and 1/3 CFD is almost perfect; ~~the~~ AL's distribution ~~instead~~, is just slightly above the others. A greater discrepancy is found for the tangential force (Fig. 6b). Here, the shapes of ~~the~~ AL, BEM and AWSM distributions are very similar to each other (owing to the ~~same polars~~ ~~fact that the same polars have been used~~), but the first shows greater values ~~from~~ ~~after~~ 25 % of the span. The lower values ~~besides~~, ~~along with~~ similar overall shapes, confirm the impact of the rotor induced velocity on the measured wind speed ahead of the turbine. A greater undisturbed velocity would indeed increase the angle of attack along the span, leading to higher values of axial and tangential forces with the same ~~distributions' shapes~~ ~~distribution shape~~, similarly to AL. Because of

Table 4. Numerical-experimental tests matrix: * exp + AL; ** exp + BEM + AWSM; *** exp + all codes. [The values of the harmonic surge frequencies \(\$f_s\$ \) and amplitudes \(\$A_s\$ \) are listed](#)

UNAFLOW #	f_s [Hz]	A_s [mm]
33**	0.125	125
37*	0.25	125
41*	0.5	65
45*	0.75	40
49*	1	50
50***	1	35
51*	1	25
53*	1.5	20
55*	1.5	10
57*	2	15
59***	2	8

the presence of the nacelle, the shape of the 1/3 CFD differs significantly from the others at the blade root, [aligning to them only until](#) around 40 % of the span. The root discrepancy does not produce any significant power variation though, since its 345 contribution to the integral torque is small.

4.2 Unsteady comparison

After having validated the [code predictions in the predictions of the codes for the](#) stationary turbine case, some of the surge 350 tests belonging to the UNAFLOW matrix have been considered, [always in RATED2 all in RATED](#) conditions (Table 2). The list of these tests is shown in Table 4, where the surge parameters are given ([in at](#) model scale) along with the corresponding wind tunnel test number. The only tests replicated by all the codes have been numbers 50 and 59.

The primary target of the unsteady experimental campaign was the characterization of the thrust force oscillation, due to its leading role in the surge dynamics of a FOWT. Indeed, the scaled model was specifically designed to match the RWT thrust coefficient. [Anyway, having the quantity Having the value](#) available from both codes and experimental measurements, [also](#) the mechanical power has been [also](#) taken into account. However, [the](#) wind tunnel torque measurements have been discovered [to be](#) affected by a mechanical resonance that biased the high frequency results. For this reason, the analysis hereinafter presented is mostly focused on the thrust. Concerning the power, only the comparison of the surge frequency harmonic is shown [, in Sect. 4.2.2, for completeness sake for the sake of completeness.](#)

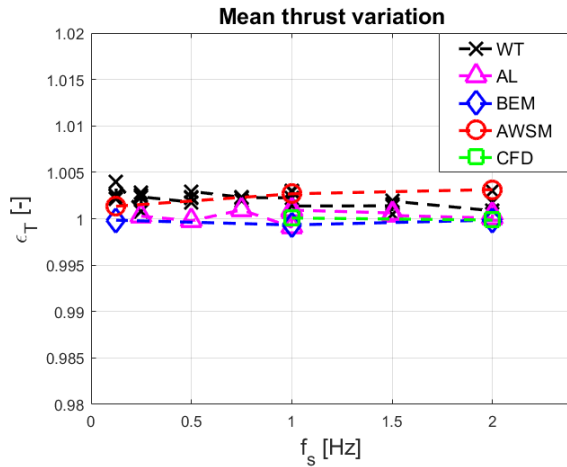


Figure 7. Mean thrust variation with the surge frequency.

4.2.1 Time domain analysis

The comparison of the thrust oscillation is first presented in the time domain, as typically found in literature. As starting point

360 of the analysis At first, the impact of the surge motion on the mean aerodynamic thrust has been assessed, since Micallef and Sant and Farrugia et al. observed a variation of the mean thrust coefficient during surge, also at the optimal λ . To check if the results are characterized by a similar behaviour, a mean thrust variation parameter can be defined as:

$$\epsilon_T = 1 + \frac{\bar{T} - T_0}{T_0}; \quad (4)$$

being with T_0 being the steady value reported in Table 3 and \bar{T} the average of the thrust signal over a full surge period. Figure 7

365 plots the values of ϵ_T , from the against the surge frequency for the different tests and simulations performed, against the surge frequency. In all the cases considered cases, the surge motion seems not does not seem to affect the mean thrust anyhow in any way. The maximum discrepancies with respect to the steady values are always below 0.5 % and utterly completely insensitive to the surge parameters. Such small variations fall within the uncertainty level associated to with each method. Therefore, for the purpose of this work, it is possible to consider $T_0 \approx \bar{T}$.

370 To continue the time domain thrust analysis, it has been decided to separate the unsteady part of the signals from the steady one, part, by subtracting the mean values from the thrust time histories. Thus considering:

$$\Delta T(t) = T(t) - T_0. \quad (5)$$

This way it is possible to avoid the steady discrepancies when comparing the time histories of different methods are considered.

375 In Fig. 8, the time histories of ΔT , obtained by the different codes, are compared to the experimental measurement and to the linear quasi-steady model prediction (Appendix A). The plot refers to the unsteady for test number 59, which has been reproduced with by all the codes (Table 4), but the. Although, similar comments apply for the other tests as well. From

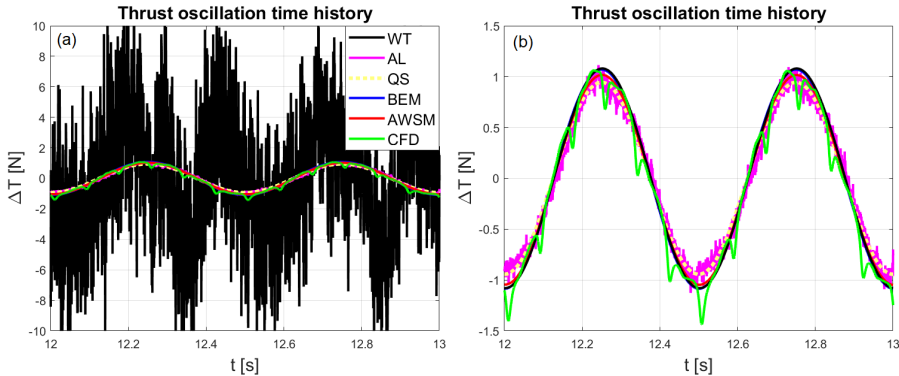


Figure 8. Thrust oscillation time histories for case 59 (a); same plot considering only the surge harmonic of wind tunnel measurements (b).

The experimental thrust time history, obtained by subtracting the inertia of the nacelle as in Eq. (2), is reported in Fig. 8. It is evident that the nacelle balance measurement was characterized by a relevant amount of disturbances, mainly caused by mechanical vibrations (e. g. platform's high frequency dynamics, imperfect surge actuation, rotordynamic effects, etc.); aerodynamic turbulence and instruments noise. Also the inertia subtraction procedure has contributed to the presence of such high frequency components, since it is effective only at . The presence of many harmonics other than the surge one is evident. The reason for this lies in the fact that the inertia subtraction works properly only on the surge harmonic. This testifies the complexity associated with the experimental investigation of the aerodynamics of a turbine subjected to imposed motions. To solve the problem, an harmonic filtering procedure has been followed. This way the wind tunnel signals have been cleaned extracting only. In fact, whilst the largest share of the surge frequency component of the balance signal (given by the very inertia of the surge frequency harmonic, getting rid of all the spurious effects nacelle) is removed, the disturbances in both balance and accelerometer signals could even be amplified depending on their relative phases (which are random). Therefore, the only meaningful harmonic after the inertia subtraction is the one at the surge frequency, and this has been extracted via a discrete Fourier Transform. Thanks to the long experimental observation periods indeed, it has been possible to get high resolution spectra despite the high sampling rate. In addition, leakage has always been avoided considering time windows lengths by taking time window lengths being integer multiples of the test surge period.

The output of this cleaning filtering procedure, applied to the thrust oscillation of test 59, is reported in Fig. 8b. The comparison reveals a very good agreement among codes, wind tunnel measurement and quasi-steady theory and wind tunnel predictions, confirming the effectiveness of extracting validity of the surge harmonic extraction from the experimental data. In fact, the different codes predictions measurements. Indeed, the numerical results appear totally dominated by the surge frequency component. In particular, BEM and AWM responses are almost purely mono-harmonic. In AL large eddy simulations instead, a certain amount of high frequency components is noticeable, but are noticeable, although insignificant with respect to the surge harmonic. The main cause of these oscillations is the turbulence that, albeit weak because of This is because, despite the smooth flow boundary condition at inlet, forms upstream the inlet, some turbulent eddies form upstream

400 of the turbine due to the turbine because of both the high wind tunnel Reynolds number ($\sim 1.6 \cdot 10^6$) and the influence of the
due to the actuator forces in the rotor plane.

Finally, the full CFD signal presents a clear component also at the blade passing frequency, due to the modelling of the turbine tower. Qualitatively, the

405 The assessment of the unsteady time histories shows a promising agreement , with the overall, with responses that often overlap with each other. Nevertheless, the time domain analysis hinders a quantitative comparison among the codes, the experiments and the quasi-steady theory because the differences are small enough to be hardly too small to be recognizable.

4.2.2 Frequency domain analysis

Having observed that the surge harmonic rules the aerodynamic response of the turbine, its frequency domain characterization becomes fundamental to validate the results. This way, the unsteady response is completely described by its amplitude and 410 phase and, and thanks to the clear reference provided by the quasi-steady theory (Appendix A), it becomes much easier to spot dynamic inflow effects due to surge. Indicating now with ΔT only the surge harmonic of the thrust oscillation, it is possible to represent it in the complex plane in terms of its amplitude and phase as:

$$\Delta T = |\Delta T| e^{i\phi} = |\Delta T| (\cos \phi + i \sin \phi); \quad (6)$$

415 being with ϕ being the phase shift between the thrust oscillation and the surge displacement at the surge frequency and i the imaginary unit. For The term $e^{i2\pi f_s t}$ has been implied in this phasor representation. For the wind tunnel measurements, the base displacement signal imposed by the surge actuator, Eq. (1), has been chosen as a phase reference. The resulting scheme is reported in Fig. 9a. For control purposes, the thrust oscillation harmonic at the surge frequency can be more conveniently expressed in terms of the states of the system, defining two coefficients of utmost importance for the surge stability assessment: 420 the-aerodynamic damping (c_{aero}) and the-aerodynamic mass (m_{aero}). Therefore, ΔT can be expressed in terms of these parameters as:

$$\Delta T = -c_{aero} \dot{x} - m_{aero} \ddot{x}; \quad (7)$$

with:

$$\dot{x} = i 2\pi f_s A_s; \quad (8)$$

$$\ddot{x} = -(2\pi f_s)^2 A_s. \quad (9)$$

425 Combining Eq. (7), (8) and (9), the expressions for the aerodynamic damping and mass coefficients are immediately derived:

$$c_{aero} = -\frac{|\Delta T| \cos \phi}{2\pi f_s A_s}; \quad (10)$$

$$m_{aero} = \frac{|\Delta T| \sin \phi}{(2\pi f_s)^2 A_s}. \quad (11)$$

In order to extend the generality of the results obtained, paving the way for a more robust comparisons ~~here and~~ also in future work, a non-dimensional characterization of the thrust oscillation harmonic at the surge frequency is proposed. For the 430 this purpose, a few non-dimensional groups have been defined. The first two are required to characterize the surge motion and have been called the *surge reduced frequency* (f_{red}) and the *surge reduced amplitude* (A_{red}), respectively. They are defined as:

$$f_{red} = \frac{f_s D}{V_0} ; \quad (12)$$

$$A_{red} = \frac{A_s}{D} ; \quad (13)$$

being D the turbine diameter and V_0 the free stream wind velocity. Note that the reduced frequency is the inverse of the reduced 435 velocity defined by Bayati et al. (2017b), and it compares the frequency of surge to ~~that associated with the characteristic one of~~ dynamic inflow, which is the most relevant source of unsteadiness associated to ~~floaters'~~ floater motions. The higher the f_{red} , the greater the chance that dynamic inflow ~~effects~~ will affect the response. The reduced amplitude ~~instead, might~~ might instead be used to evaluate the validity boundaries of the small ~~displacements~~ displacement assumption required to get the linear quasi-steady model (Appendix A).

440 To fully characterize the surge harmonic of the thrust response, its phase has been used ~~directly, whilst as it is, while~~ for the amplitude an *unsteady thrust coefficient* ($C_{\Delta T}$) has been defined following the steady thrust coefficient definition:

$$C_{\Delta T} = \frac{|\Delta T|}{0.5 \rho A_D V_0^2} ; \quad (14)$$

being ~~with~~ ρ being the air density and A_D the area of the disk swept by the blades. Relying on the quasi-steady assumption, Eq. (A5) can be reworked ~~letting~~, letting the non-dimensional groups to appear so that an expression for the unsteady thrust 445 coefficient is found:

$$C_{\Delta T} = 2\pi c_0^* f_{red} A_{red} . \quad (15)$$

The coefficient c_0^* has been derived from the nondimensionalization of Eq. (A7) and it has been called *non-dimensional steady aerodynamic damping*. The ~~An~~ interesting fact is that it is only a function of the steady thrust coefficient curve of the turbine $C_T(\lambda)$, in fact:

$$450 \quad c_0^* = \frac{c_0}{0.5 \rho A_D V_0} = 2C_T(\lambda_0) - \frac{dC_T}{d\lambda}|_{\lambda_0} \cdot \lambda_0 ; \quad (16)$$

being ~~with~~ λ_0 being the steady operating conditions tip speed ratio and c_0 the steady aerodynamic damping defined in Appendix A.

Exploiting the new variables, the ~~results comparison~~ comparison of the results is presented in a non-dimensional form. In Fig. 9b, the amplitude of the thrust oscillation at the surge harmonic is characterized, plotting the ratio between the unsteady 455 thrust coefficient and the reduced surge amplitude against the ~~surge reduced reduced surge~~ frequency. The reason behind this choice is the linear trend foreseen by the quasi-steady theory, i.e. Eq. (15), that provides a clear theoretical reference for the comparison. It is worth to note that the slope of the quasi-steady reference has been evaluated analytically using

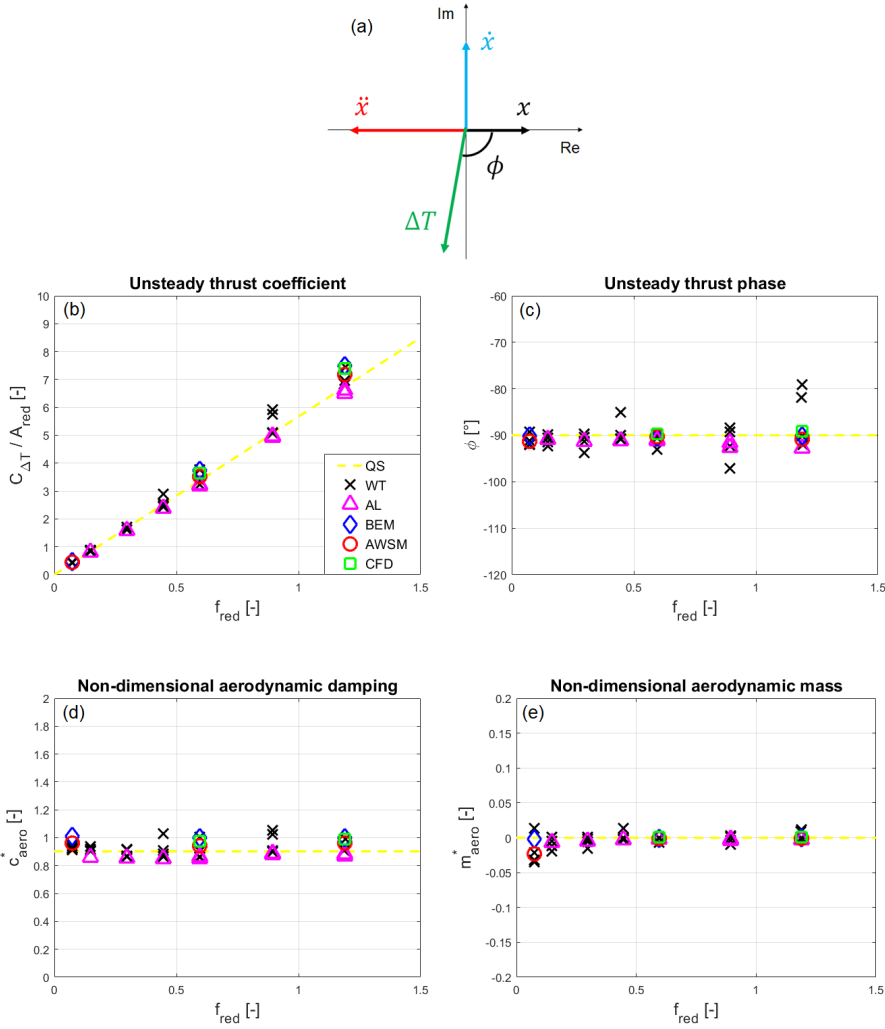


Figure 9. Complex representation of the [thrust oscillation's surge harmonic](#) [of the thrust oscillation](#) (a); unsteady thrust coefficient comparison (b); comparison of the phase of the [surge harmonic](#) of the thrust oscillation [is surge harmonic](#) (c); aerodynamic damping comparison (d); aerodynamic mass comparison (e).

the RWT characteristic curve, as explained in Appendix A. The plot reveals an excellent agreement among all the codes involved and [the](#) wind tunnel tests, with a maximum deviation [of](#) around 10 % at the highest reduced frequency. Anyway, 460 all the numerical predictions fall inside the experimental [tests scatter](#). [Diversely from test](#) scatter. [In contrast to](#) the steady turbine case, BEM, CFD and AWSM tend to predict slightly higher values than [AL and the AL](#) and the analytical model, with wind tunnel measurements typically in between. [Although, all All](#) the data seem to confirm the linear trend predicted with the quasi-steady assumption.

The comparison in terms of phase of ΔT is shown in Fig. 9c. According to the reference system of Fig. 3b, the quasi-steady
465 model foresees ΔT to be in opposition of phase with respect to the surge velocity. Having referred the phase to the surge
displacement, the reference value is then $\phi = -90^\circ$. Once again, the codes agree closely with the quasi-steady theory, with
discrepancies just slightly increasing with f_{red} . The phase values from the wind tunnel tests instead show a relevant scatter
because of the uncertainty entailed by the inertia subtraction procedure. Especially at high frequencies indeed, the share of
470 the aerodynamic thrust in the balance measurement is much smaller than the inertial contribution due to surge acceleration
and the surge acceleration. As a result, when the subtraction is performed, the phase of ΔT appears much more sensitive to
disturbances than its amplitude (Mancini, 2020).

Knowing amplitude and the amplitude and the phase of the thrust oscillation's surge harmonic surge harmonic of the thrust
oscillation, it is possible to evaluate the aerodynamic mass and damping coefficients from Eq. (10) and (11). To continue with
a non-dimensional analysis, the non-dimensional aerodynamic damping coefficient (c_{aero}^*) and the non-dimensional aerody-
475 namic mass coefficient (m_{aero}^*) have been defined as:

$$c_{aero}^* = \frac{c_{aero}}{0.5 \rho A_D V_0} ; \quad (17)$$

$$m_{aero}^* = \frac{m_{aero}}{\rho A_D D} . \quad (18)$$

According to the quasi-steady theory, $c_{aero}^* = c_0^*$ and $m_{aero}^* = 0$. The non-dimensional comparison in terms of aerodynamic
damping is reported in Fig. 9d. All the codes show a constant trend with respect to the reduced frequency, confirming the linear-
480 ity of the plot in Fig. 9b and thus the validity of the quasi-steady assumption. Concerning the non-dimensional aerodynamic
mass, Fig. 9e confirms that its values are always extremely close to zero, in agreement with the quasi-steady theory. Only a
slight scatter appears at the lowest frequencies because of the inverse dependency of m_{aero} on the square of f_s , as shown in
Eq. (11); this amplifies even very small phase errors, leading to unphysical values of the aerodynamic mass.

Very similar considerations to those regarding the thrust can be made for the power oscillation. In particular, being as the
485 unsteady response is dominated by the surge harmonic, it is convenient to characterize it in the frequency domain. Similarly to
the thrust, it is possible to represent the power oscillation's surge harmonic surge harmonic of the power oscillation (ΔP) in
the complex plane as:

$$\Delta P = |\Delta P| e^{i\phi_P} = |\Delta P| (\cos \phi_P + i \sin \phi_P) ; \quad (19)$$

being with ϕ_P being the argument of ΔP , always with respect to the surge displacement harmonic, and again implying the
490 term $e^{i2\pi f_s t}$. Differently from the thrust case, the expression of the power oscillation in terms of the system's system states is
avoided since ΔP does not affect the stability, but only only affects the power harvesting. Passing in, not the system stability.
To pass to a non-dimensional form, it is possible to define the unsteady power coefficient ($C_{\Delta P}$) as:

$$C_{\Delta P} = \frac{|\Delta P|}{0.5 \rho A_D V_0^3} . \quad (20)$$

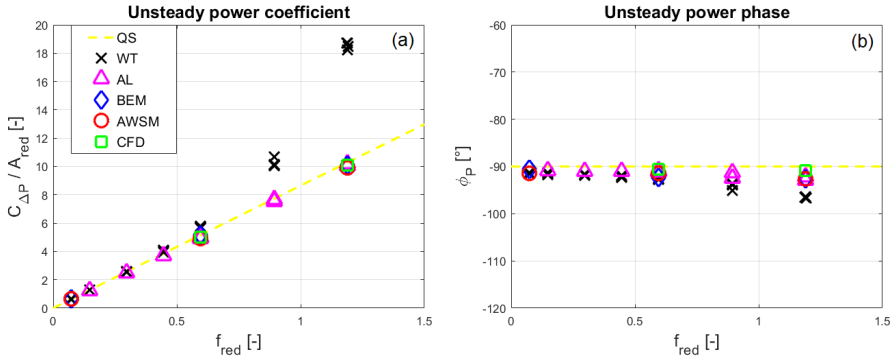


Figure 10. Unsteady power coefficient comparison (a); comparison of the phase of the surge harmonic of the power oscillation is surge harmonic (b).

Then, reworking Eq. (A6), a non-dimensional expression linking the unsteady power coefficient to the steady turbine is operating conditions and to the surge parameters can be found, again relying on the quasi-steady assumption:

$$C_{\Delta P} = 2\pi \zeta_0^* f_{red} A_{red} . \quad (21)$$

Latter The latter expression perfectly corresponds to Eq. (15) concerning the thrust. Only this time This time though, the parameter depending on the turbine is steady performance is ζ_0^* , rather than c_0^* , and it is defined as:

$$\zeta_0^* = \frac{\zeta_0}{0.5 \rho A_D V_0^2} = 3 C_P(\lambda_0) - \frac{dC_P}{d\lambda} |_{\lambda_0} \cdot \lambda_0 ; \quad (22)$$

being with C_P the turbine's being the turbine power coefficient and ζ_0 the parameter defined in Eq. (A8), which links the power oscillation to the surge velocity.

The comparison in terms of the unsteady power coefficient is reported in Fig. 10a, always dividing by the reduced surge amplitude and plotting it against the reduced frequency to have a linear quasi-steady reference. As previously anticipated, the torque measured by the balances in the wind tunnel tests was subjected to a dynamic effect altering the power oscillation in the higher frequency cases. In fact, the sharp amplitude increase arising as soon as f_s exceeded 1 Hz, and the contextual phase reduction (Fig. 10b) were caused by a powertrain resonance standing at 3.95 Hz. As long as the natural frequency was far, the angular degree of freedom behaved quasi-statically with respect to such a vibration mode and the results were almost unaffected; getting closer to the resonance, the a typical mechanical amplification phenomenon occurred. As a result, only the low f_{red} cases have been validated by the wind tunnel measurements. However, the excellent agreement among all the codes and the quasi-steady model gives a great confidence on the numerical results' validity great confidence in the validity of the numerical results regarding ΔP for the whole frequency range. The quasi-steady behaviour found is also totally coherent to what consistent with what has been observed for the thrust, in which the codes' predictions have been confirmed by the experiments. If new unsteady tests will be conducted, some stiffness will be added to the angular degree of freedom (e.g. changing the transmission belt) in order to move the resonance farther from the f_s range considered.

515 The phase comparison is reported in Fig. 10b and it confirms the conclusions of the unsteady power coefficient case. Leaving the wind tunnel measurements aside, the codes show little few discrepancies among each other. Nevertheless, a reduction of ϕ_P with respect to the quasi-steady value appears to occur at the higher frequencies, resembling a dynamic inflow effect. A similar reduction has also been found by the actuator line in the phase of the thrust, with the other codes showing values closer to -90° . In the power case, the codes seem to be more concordant in among each other about the presence of this slight delay.
520 However, no matter which code is considered, the maximum phase shift with respect to the quasi-steady reference is always below three degrees and thus negligible. As for the amplitude plot, the low frequency wind tunnel tests utterly fully confirm the numerical outcomes, whilst a phase shift due to the resonance affects the higher f_{red} results.

5 Conclusions

525 The performance response to an harmonic surge motion harmonic surge motions of a 1:75 scaled version of the DTU10MW RWT has been investigated using state-of-art state-of-the-art numerical models with different fidelity levels. For the first time, the unsteady results have been validated against high fidelity wind tunnel tests specifically focused on the aerodynamics. These tests, in which the surge motion was imposed to the scaled turbine, were conducted in Polimi's facility (GVPM) within the UN-AFLOW project. The comparison has revealed a surprisingly good agreement among the different codes' predictions predictions of the different codes, with smaller discrepancies in the unsteady case than the steady one. The codes have all confirmed the 530 aerodynamic response to be dominated by the component at the surge frequency. Hence, considering only that harmonic, it has been possible to clean the experimental measurements that were characterized by significant disturbances due to the unsteady tests' complexity complexity of the unsteady tests. The resulting thrust measurements have validated the codes' predictions for the whole test matrix. Concerning the torque instead, the experiments have been able to confirm only the low frequency outcomes, since the higher frequency signals were biased by a mechanical resonance. However, the excellent numerical results' 535 agreement agreement of the numerical results suggests the validity of the codes' predictions also for the unsteady power.

Owing to its leading role in the aerodynamic response, the surge harmonic has been characterized in the frequency domain. This has allowed to perform a more quantitative comparison of the unsteady results, at the same time focusing on control relevant parameters. The analysis has been presented in a non-dimensional form, aiming to maximize its generality. The focus on the surge harmonic has given the possibility to define a linear analytical model, based on the quasi-steady assumption, 540 with which both numerical and experimental results have been further validated. Despite the several approximations made, the quasi-steady model has shown an outstanding match with the other data, allowing to confirm the the confirmation of conclusions drawn by de Vaal et al. (2014), so that the aerodynamic response of a floating wind turbine at rated wind conditions to typical wave induced surge motions can be well-modelled relying on at rated wind conditions can be well-modelled with the quasi-steady assumption. In the conditions considered indeed, the rotor unsteadiness has had little influence on the loads and even the 545 BEM code has produced accurate results using a classical dynamic inflow model. The absence of mean performance variations due to surge has been an ulterior proof corroborating this evidence. Nevertheless, such a conclusion is tightly linked to the frequency range selected, as well as to the specific time scale of dynamic inflow. In fact, f_{red} is the parameter that rules the

impact of dynamic inflow effects. In this work, its values have not exceeded 1.2, but the increasing ~~results scatter towards scatter of the results with~~ higher frequencies likely indicates the inception of unsteady effects. The results presented have revealed 550 that the accuracy of the quasi-steady assumption is almost insensitive to the surge reduced amplitude. ~~Although~~However, it should be verified up to what threshold non-linear effects can be neglected and the small displacements assumption holds. ~~Anyhow~~Regardless, the size of the rotors currently employed in offshore wind farms ~~warrants~~arouses little concern about the magnitude of A_{red} .

The linear quasi-steady model proposed, expressed in non-dimensional terms, might be a convenient tool ~~also for future work~~for future works as well. As long as a similar reduced frequency range is considered~~indeed, the loads~~, the load oscillation amplitudes can be effectively estimated by means of Eq. (15) and (21), whilst the phase can be reasonably assumed equal to the quasi-steady reference. This approach separates the influence of the surge parameters from that of the steady operating conditions, allowing to better understand the impact that each single variable has on the unsteady behaviour. Furthermore, its integral load perspective makes it suitable for control strategy design and assessment. For example, the increase of the ~~leads~~ oscillation amplitudes~~load oscillation amplitudes~~, found by Micallef and Sant (2015) raising the tip speed ratio at constant A_s and f_s , may be explained by an increase of both c_0^* and ζ_0^* linked to the steady characteristic curves ~~z~~-shapes that, of course, depend on the controller. Moreover, the critical operating points where the stability is in jeopardy because of small (or negative) aerodynamic damping can be immediately found from the expression ~~of~~for c_0^* . Then, the control strategy can be adjusted to modify the steady characteristic curves, adding some more surge damping where needed. In fact, a higher c_0^* means a higher 560 $C_{\Delta T}$ only if the surge is assumed imposed in Eq. (15); in reality, a higher damping would drastically reduce A_{red} , ~~providing a benefit overall~~providing overall benefit.

In future ~~work~~works, higher reduced frequency cases where dynamic inflow effects appear will be addressed to understand what happens when the quasi-steady assumption ~~falls~~. ~~The codes~~The code validation effort hereby described has increased the confidence on the numerical predictions~~indeed~~, paving the way for ~~considering~~the consideration of more critical 570 cases. A similar characterization will be also attempted for the turbine pitch case, which is expected to be more challenging due to the radial variation of the imposed motion. Finally, a revision of the powertrain assembly is being carried out to make sure that, if new unsteady experiments ~~had~~have to be conducted, the torque measurements would not be affected by any resonance.

Data availability. All the data presented in this work are stored in a FTP server, together with the whole UNAFLOW database. Upon request the access keys will be granted out of charges to anyone interested.

575 Appendix A: Linear quasi-steady model

Exploiting the quasi-steady assumption, it is possible to obtain a theoretical reference for the unsteady ~~performances~~performance of a turbine subjected to surge. In fact, as long as the motion period is long compared to the time scale of dynamic inflow, i.e. the reduced frequency of Eq. (12) is small, the induction field can be assumed to adjust immediately to the relative wind change

imposed by ~~surge~~ the surge motion. If dynamic stall effects are neglected, the hypothesis of no dynamic inflow automatically 580 implies the absence of airfoil unsteadiness, since it occurs at a shorter time scale larger time scales. Thus, assuming a quasi-steady behaviour, the turbine ~~performances~~ performance can be expressed in terms of the thrust and power coefficients, and the surge motion reduces to a change of the incoming wind speed experienced by the rotor (V_w). In particular:

$$V_w = V_0 - \dot{x}; \quad (A1)$$

having used using the reference system of Fig. 3b. This modifies the expression of the tip speed ratio that becomes to become:

$$585 \quad \lambda_w = \frac{\Omega D}{2 V_w}. \quad (A2)$$

Consequently, the turbine ~~'s~~ thrust and power responses can be expressed as:

$$T = \frac{1}{2} \rho A_D C_T(\lambda_w) V_w^2; \quad (A3)$$

$$P = \frac{1}{2} \rho A_D C_P(\lambda_w) V_w^2. \quad (A4)$$

To obtain the easy reference used in the paper, the expressions have been linearized for small surge velocities, i.e. $\dot{x} \rightarrow 0$. 590 In case of harmonic surge ~~displacement~~ displacements, this can be translated to a condition on the reduced surge amplitude $A_{red} \rightarrow 0$, which means $A_s \ll D$. Hence, the linear approximation is likely to be suitable for modern multi-megawatt rotors employed in floating wind farms. Considering small variations around the steady operating conditions and a constant rotational speed (as in the wind tunnel tests) the following expressions for the thrust and power oscillations have been obtained:

$$\Delta T \approx -c_0 \dot{x}; \quad (A5)$$

$$595 \quad \Delta P \approx -\zeta_0 \dot{x}; \quad (A6)$$

with c_0 and ζ_0 functions only of the steady operating conditions of the turbine, defined as:

$$c_0 = -\frac{dT}{d\dot{x}}|_{\dot{x}=0} = \frac{1}{2} \rho A_D [2 V_0 C_T(\lambda_0) - \frac{dC_T}{d\lambda}|_{\lambda_0} \frac{\Omega D}{2}]; \quad (A7)$$

$$\zeta_0 = -\frac{dP}{d\dot{x}}|_{\dot{x}=0} = \frac{1}{2} \rho A_D V_0 [3 V_0 C_P(\lambda_0) - \frac{dC_P}{d\lambda}|_{\lambda_0} \frac{\Omega D}{2}]. \quad (A8)$$

By means of this simplified approach, it is possible to estimate the unsteady response knowing the steady operating point, the 600 characteristic curves and the surge motion parameters. Provided that the ~~sealed model's~~ complete characteristic curves of the scaled model were unavailable, those of the RWT have been used. The in this work. In fact, the scaled turbine was designed to match the DTU10MW ~~RWT thrust coefficient indeed thrust coefficient~~, but also the power coefficient was well reproduced in rated conditions (Bayati et al., 2017a). Although, the RWT performance curves, however, take into account also the regulation the regulation as well, whilst in the experimental campaign both the rotational speed and the blades pitch were kept 605 constant. To bypass this issue, the shapes of the curves in the neighbourhood of $\lambda = 7.5$ have been approximated taking three points where the regulation has little or ~~none~~ no influence, fitting them with a quadratic trend. Except from that at curve. Except

for one at the optimal tip speed ratio, the other two points have been selected as close as possible to the first, but towards with higher λ (i.e. $\lambda = 8$ and 9.3). In the below-rated region, not too far from $\lambda = 7.5$, the pitch regulation is very small in fact indeed and the rotational speed stays constant at the its minimum value. Such a procedure had to be followed for evaluating to evaluate c_0 , whilst for ζ_0 the derivative of C_P at the optimal tip speed ratio is obviously close to zero and thus the knowledge of $C_P(\lambda_0)$ is enough. Despite its simplicity, this approach can provide accurate predictions as long as: the quasi-steady assumption holds (i.e. $f_{red} \rightarrow 0$ thus $f_s \ll V_0/D$), the surge velocity is small (i.e. $A_{red} \rightarrow 0$ thus $A_s \gg D$; $A_s \ll D$), and the right characteristic curves are used (i.e. if the regulation is active during surge the curves have to take it into account or vice versa). Finally, it is worth to notice that also a variable rotational speed might be considered also be considered, adding little complication to the model.

Author contributions. S. Mancini conducted the UNAFLOW project revision, run the actuator line simulations and coordinated the manuscript composition under the supervision of A. Zasso and P. Schito. K. Boorsma and M. Caboni performed BEM and AWSM simulations, while M. Cormier and T. Lutz provided the CFD results. All the authors contributed with their ideas and thoughts to the development of the paper.

Competing interests. The authors declare that they have no conflict of interest.

620 *Acknowledgements.* This research has been funded by EU-EERA (European Energy Research Alliance)/IRPWIND Joint Experiment 2017. The authors gratefully acknowledge HLRS Stuttgart and Cineca HPC for providing computational resources.

References

- Bayati, I., Belloli, M., Bernini, L., and Zasso, A.: Wind tunnel validation of AeroDyn within LIFES50+ project: imposed Surge and Pitch tests, *J. Phys.: Conf. Ser.*, 753, <https://doi.org/10.1088/1742-6596/753/9/092001>, 2016.
- 625 Bayati, I., Belloli, M., Bernini, L., Giberti, H., and Zasso, A.: Scale model technology for floating offshore wind turbines, *IET Renew. Power Gener.*, 11, 1120–1126, <https://doi.org/10.1049/iet-rpg.2016.0956>, 2017a.
- Bayati, I., Belloli, M., Bernini, L., and Zasso, A.: Wind Tunnel Wake Measurements of Floating Offshore Wind Turbines, *Energy Procedia*, 137, 214–222, <https://doi.org/10.1016/j.egypro.2017.10.375>, 2017b.
- 630 Bayati, I., Belloli, M., Bernini, L., and Zasso, A.: Aerodynamic design methodology for wind tunnel tests of wind turbine rotors, *Renewable Energy*, 167, 1–12, <https://doi.org/10.1016/j.jweia.2017.05.004>, 2017c.
- Bayati, I., Belloli, M., Bernini, L., Boldrin, D. M., Boorsma, K., Caboni, M., Cormier, M., Mikkelsen, R., Lutz, T., and Zasso, A.: UNAFLOW project: UNsteady Aerodynamics of FLOating Wind turbines, *J. Phys.: Conf. Ser.*, 1037, <https://doi.org/10.1088/1742-6596/1037/7/072037>, 2018a.
- 635 Bayati, I., Bernini, L., Zanotti, A., Belloli, M., and Zasso, A.: Experimental investigation of the unsteady aerodynamics of FOWT through PIV and hot-wire wake measurements, *J. Phys.: Conf. Ser.*, 1037, <https://doi.org/10.1088/1742-6596/1037/5/052024>, 2018b.
- Bernini, L., Bayati, I., Boldrin, D. M., Cormier, M., Caboni, M., and Mikkelsen, R. F.: UNsteady Aerodynamics for Floating Wind (UN-AFLOW), Report, Politecnico di Milano, Milan, Italy, 2018.
- Boorsma, K., Grasso, F., and Holierhoek, J. G.: Enhanced approach for simulation of rotor aerodynamic loads, Report ECN-M-12-003, ECN, presented at EWEA Offshore 2011, Amsterdam, 29 November 2011 - 1 December 2011, 2011.
- 640 Boorsma, K., Hartvelt, M., and Orsi, L. M.: Application of the lifting line vortex wake method to dynamic load case simulations, *J. Phys.: Conf. Ser.*, 753, <https://doi.org/10.1088/1742-6596/753/2/022030>, 2016.
- Boorsma, K., Wenz, F., Lindenburg, C., Aman, M., and Kloosterman, M.: Validation and accommodation of vortex wake codes for wind turbine design load calculations, *Wind Energ. Sci. Discuss.*, <https://doi.org/10.5194/wes-2020-6>, 2020.
- 645 Cormier, M., Caboni, M., Lutz, T., Boorsma, K., and Krämer, E.: Numerical analysis of unsteady aerodynamics of floating offshore wind turbines, *J. Phys.: Conf. Ser.*, 1037, <https://doi.org/10.1088/1742-6596/1037/7/072048>, 2018.
- de Vaal, J. B., Hansen, M. O. L., and Moan, T.: Effect of wind turbine surge motion on rotor thrust and induced velocity, *Wind Energ.*, 17, 105–121, <https://doi.org/10.1002/we.1562>, 2014.
- Farrugia, R., Sant, T., and Micallef, D.: Investigating the aerodynamic performance of a model offshore floating wind turbine, *Renewable Energy*, 70, 24–30, <https://doi.org/10.1016/j.renene.2013.12.043>, 2014.
- 650 Farrugia, R., Sant, T., and Micallef, D.: A study on the aerodynamics of a floating wind turbine rotor, *Renewable Energy*, 86, 770–784, <https://doi.org/10.1016/j.renene.2015.08.063>, 2016.
- Goupee, J. A., Kimball, R. W., and Dagher, H. J.: Experimental observations of active blade pitch and generator control influence on floating wind turbine response, *Renewable Energy*, 104, 9–19, <https://doi.org/10.1016/j.renene.2016.11.062>, 2017.
- Jameson, A., Schmidt, W., and Turkel, E.: Numerical solution of the Euler equations by finite volume methods using Runge Kutta time stepping schemes, in: 14th fluid and plasma dynamics conference, p. 1259, Palo Alto, CA, USA, 1981.
- 655 Khosravi, M., Sarkar, P., and Hu, H.: An Experimental Investigation on the Performance and the Wake Characteristics of a Wind Turbine Subjected to Surge Motion, in: 33rd Wind Energy Symposium 2015/AIAA SciTech Forum 2015, AIAA 2015-1207, Kissimmee, Florida, <https://doi.org/10.2514/6.2015-1207>, 2015.

- Kowarsch, U., Keßler, M., and Krämer, E.: High order CFD-simulation of the rotor-fuselage interaction, in: 44th European Rotorcraft Forum, 660 Moscow, Russia, 2013.
- Kroll, N. and Faßbender, J. K.: MEGAFLOW - Numerical Flow Simulation for Aircraft Design, Springer Verlag, 2005.
- Lennie, M., Marten, D., Pechlivanoglou, G., Nayeri, C. N., and Paschereit, C. O.: Modern methods for investigating the stability of a pitching floating platform wind turbine, *J. Phys.: Conf. Ser.*, 753, <https://doi.org/10.1088/1742-6596/753/8/082012>, 2016.
- Lindenburg, C. and Schepers, J. G.: Phatas-IV Aeroelastic Modelling, Release 'DEC-1999' and 'NOV-2000', Report ECN-CX-00-027, 665 ECN, 2000.
- Madsen, F. J., Nielsen, T. R. L., Kima, T., Bredmose, H., Pegalajar-Jurado, A., Mikkelsen, R. F., Lomholt, A. K., Borg, M., Mirzaei, M., and Shin, P.: Experimental analysis of the scaled DTU10MW TLP floating wind turbine with different control strategies, *Renewable Energy*, 155, 330–346, <https://doi.org/10.1016/j.renene.2020.03.145>, 2020.
- Mancini, S.: An Experimental, Analytical and Numerical Study of FOWT's Unsteady Aerodynamics, M.s. thesis, Politecnico di Milano, 670 Milan, Italy, 2020.
- Mantha, D., Schlipf, M., Cordle, A., Pereira, R., and Jonkman, J.: Challenges in Simulation of Aerodynamics, Hydrodynamics, and Mooring-Line Dynamics of Floating Offshore Wind Turbines, in: 21st Offshore and Polar Engineering Conference, Maui, Hawaii, 2011.
- Melani, P. F., Schito, P., and Persico, G. B. A.: Experimental Assessment of an Actuator-Line Simulation Tool for VAWTs, in: Wind Energy Exploitation in Urban Environment. TURbWind 2018, edited by Battisti, L., pp. 177–200, Springer International Publishing, Milan, Italy, 675 https://doi.org/10.1007/978-3-030-13531-7_11, 2019.
- Menter, F. R.: Two-equation eddy-viscosity turbulence models for engineering applications, *AIAA journal*, 32, 1598–1605, 1994.
- Micallef, D. and Sant, T.: Loading effects on floating offshore horizontal axis wind turbines in surge motion, *Renewable Energy*, 83, 737–748, <https://doi.org/10.1016/j.renene.2015.05.016>, 2015.
- Nielsen, F. G., Hanson, T. D., and Skaare, G.: Integrated dynamic analysis of floating offshore wind turbines, in: Proceedings of the 25th 680 International Conference on Offshore Mechanics and Arctic Engineering, pp. 671–679, Hamburg, Germany, 2006.
- Pedersen, M. D.: Stabilization of Floating Wind Turbines, Ph.d thesis, NTNU, Trondheim, Denmark, 2017.
- Ren, N., Li, Y., and Ou, J.: Coupled wind-wave time domain analysis of floating offshore wind turbine based on Computational Fluid Dynamics method, *J. Renew. Sustain. Ener.*, 6, <https://doi.org/10.1063/1.4870988>, 2014.
- Sant, T., Bonnici, D., Farrugia, R., and Micallef, D.: Measurements and modelling of the power performance of a model floating wind turbine 685 under controlled conditions, *Wind Energ.*, 18, 811–834, <https://doi.org/10.1002/we.1730>, 2015.
- Sarlak, H., Meneveau, C., and Sørensen, J. N.: Role of subgrid-scale modeling in large eddy simulation of wind turbine wake interactions, *Renewable Energy*, 77, 386–399, <https://doi.org/10.1016/j.renene.2014.12.036>, 2015.
- Sayed, M., Lutz, T., and Krämer, E.: Aerodynamic investigation of flow over a multi-megawatt slender bladed horizontal-axis wind turbine, in: Renewable Energies Offshore, pp. 773–780, Lisbon, Portugal, 2015.
- Schito, P.: Large Eddy Simulation of wind turbines: interaction with turbulent flow, Ph.d thesis, Politecnico di Milano, Milan, Italy, 690 2011.
- Schito, P. and Zasso, A.: Actuator forces in CFD: RANS and LES modeling in OpenFOAM, *J. Phys.: Conf. Ser.*, 524, <https://doi.org/10.1088/1742-6596/524/1/012160>, 2014.
- Schito, P., Bayati, I., Belloli, M., Bernini, L., Dossena, V., and Zasso, A.: Numerical Wind Tunnel Tests of an Open Data IPC-VAWT, in: Wind Energy Exploitation in Urban Environment. TURbWind 2017, edited by Battisti, L. and Ricci, M., pp. 113–122, Springer, Cham, 695 Milan, Italy, https://doi.org/10.1007/978-3-319-74944-0_8, 2018.

- Sebastian, T. and Lackner, M. A.: Analysis of the Induction and Wake Evolution of an Offshore Floating Wind Turbine, *Energies*, 5, 968–1000, <https://doi.org/10.3390/en5040968>, 2012.
- Sebastian, T. and Lackner, M. A.: Characterization of the unsteady aerodynamics of offshore floating wind turbines, *Wind Energ.*, 16, 339–352, <https://doi.org/10.1002/we.545>, 2013.
- 700 Snel, H.: Heuristic modelling of dynamic stall characteristics, in: Conference proceedings European Wind Energy Conference, pp. 429–433, Dublin, Ireland, 1997.
- Snel, H. and Schepers, J. G.: JOULE1: Joint investigation of Dynamic Inflow Effects and Implementation of an Engineering Model, Report ECN-C-94-107, ECN, 1994.
- Snel, H., Houwink, R., van Bussel, G. J. W., and Bruining, A.: Sectional prediction of 3D effects for stalled flow on rotating blades and 705 comparison with measurements, in: Proc. European Community Wind Energy Conference, Travemünde, Germany, 1993.
- Tran, T. T. and Kim, D. H.: A CFD study into the influence of unsteady aerodynamic interference on wind turbine surge motion, *Renewable Energy*, 90, 204–228, <https://doi.org/10.1016/j.renene.2015.12.013>, 2016.
- van Garrel, A.: Development of a Wind Turbine Aerodynamics Simulation Module, Report ECN-C-03-079, ECN, 2003.
- Øye, S.: A simple vortex model of a turbine rotor, in: Proceedings of the third IEA symposium on the aerodynamics of wind turbines, pp. 710 1–15, Harwell, UK, 1990.